Wetropolis rainfall and flood demonstrator: towards real-time simulations with data assimilation

Tom Kent and Onno Bokhove
School of Mathematics, University of Leeds, U.K.

Abstract

[From DARE proposal:] The Wetropolis flood demonstrator is a conceptual physical model that illustrates how extreme hydroclimatic events can cause flooding of a city due to peaks in river levels and groundwater following intense rainfall. It aims to conceptualise the science of flooding in a way that is accessible to and directly engages the public; furthermore, it offers great potential as a scientific testbed for flood modelling, mitigation, control, and data assimilation. This study aims (i) to exploit this potential for the first time by improving the numerical modelling and introducing a data assimilation component; and (ii) to enhance the use of Wetropolis as an engaging outreach tool by providing a display of real-time simulations. Since Wetropolis' inception, there has been demand from stakeholders and scientists, including recently from Leeds Institute of Fluid Dynamics, for a full predictive numerical model in order to facilitate a live display of the numerical simulations in tandem with the physical set-up. We have established (i) a hydrodynamic model, which is more realistic than the original design model, and (ii) a graphical dashboard for visualising the numerical simulations of the full Wetropolis system. To enhance the predictive capability, it is necessary to constrain the model using data; this is carried out in two stages. First, we conduct identical twin experiments using an ensemble Kalman filter to update the water levels and estimate the (one or more unknown) parameters of the system. Once this framework has been established, we work towards assimilating real data provided by water-level measuring devices placed at a number of locations along the river channel. On completion of this second stage, credible real-time simulations can be displayed alongside the physical set-up, and thereby offer an enriched experience to viewers of Wetropolis. An interesting next stage is to explore strategies for real-time flood control and monitoring via model-predictive control (MPC); the output from this study facilitates further research in this direction.

1 Introduction

Urban flooding is a major hazard worldwide, brought about by intense rainfall and often exacerbated by the built environment. The tabletop flood-demonstrator 'Wetropolis' illustrates in an idealised modelling environment how extreme hydroclimatic events can cause flooding of a city due to peaks in river levels and groundwater following intense rainfall. It aims to conceptualise the science of flooding in a way that is accessible to and directly engages the

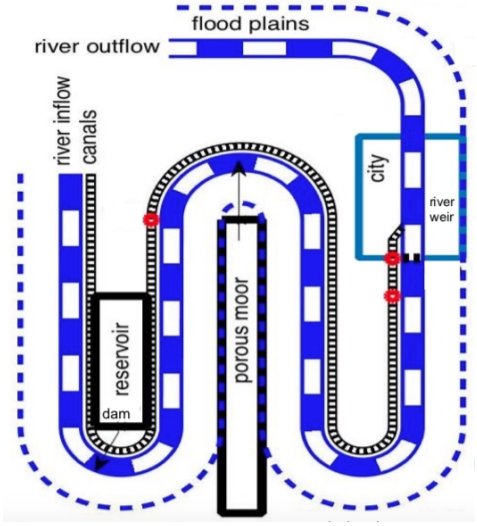

Figure 1: Plan view of Wetropolis showing the winding river channel... [Bokhove et al., 2020].

public and also provides a scientific testbed for flood modelling, control and mitigation, and data assimilation. As such, it is useful to the scientist, industrial practitioner, and general public.

Physically, it comprises a winding river channel with parallel canal, a reservoir for water storage, a porous flow cell (analogous to a moor) with observable groundwater level and flow, and random "rainfall", which may or may not lead to flooding in the idealised urban area of Wetropolis. The main river channel has three π–degree bends and one $(\pi/4)$–degree bend, and is fed by water flowing into the domain at an upstream entry and leaving the domain at the downstream exit. The river bed is sloping down (uniformly with gradient 1 in 100); the river cross-sectional area is rectangular and uniform, and flanked on one side by a sloping flood plain outside of the urban area. Through the urban area, the rectangular channel is flanked on both sides by flat rectangular plains of higher elevation than the regular river channel, i.e., the cross-sectional area is T-shaped.

Water enters the main channel in three places: (i) at the upstream end where inflow is generally kept constant; (ii) from a groundwater cell (or "moor") with porous material, fed by random daily rainfall and with flow down into the river via an outlet (canal); and (iii) via an overflow from a reservoir or "lake", also fed by random daily rainfall. The moor and reservoir components can be placed in three different locations along the river channel: on the upstream, midstream, or downstream bends. A schematic of the set-up with the reservoir and moor at the upstream and midstream locations, respectively, is displayed in Fig. 1.

Rainfall is supplied randomly in space at four locations (reservoir, moor, reservoir and moor, or nowhere) and randomly in time at four rainfall rates corresponding to 10%, 20%, 40%, or 90% of a Wetropolis day (wd) according to two skew-symmetric discrete probability distributions. The joint probabilities (rain amount times rain location) are determined daily

as one of 16 possible outcomes from two separate or aligned asymmetric Galton boards, in which a steel ball or two such balls descend through the Galton boards every wd and according to the corresponding discrete probability distributions. The most extreme daily rainfall event thus involves rainfall on both moor and reservoir for 90% of a Wetropolis day.

Wetropolis' design was based originally on simulations of a one-dimensional numerical model of the dynamics that uses a kinematic approximation to describe the river flow and a depth-averaged nonlinear diffusion equation for the groundwater cell; in the numerical model, a stochastic rainfall generator determines the amount and location of rain per wd. In order to create an extreme flood event in Wetropolis once every 5 to 10 minutes on average instead of, say, once every 100 to 200 years on average (as for an actual river), the length of the Wetropolis day was chosen a priori to be 10s; preliminary modelling then determined the approximate value of other parameters such that flooding in the city region generally follows "extreme rainfall" in the catchment. Conceptualising and communicating the notion of a return period, often misunderstood by non-specialists, was the main motivation for Wetropolis' design and construction. Thus, Wetropolis is able to demonstrate random extreme rainfall and flood events in a physical model on reduced spatial and temporal scales. See Bokhove et al. [2020] for more details, including that Wetropolis' return period is (256/7) x 10s = 6:06min

The numerical design model therein, based on the equations for open channel flow (cf. Chanson [2004]), is used to determine the relevant time and length scales prior to its construction as a physical model. That is, it is a crude and inexpensive model suitable for design purposes. Here, we develop the hydrodynamic modelling further, both mathematically and numerically, and improve the visualisation of its output, with a view to conducting real-time simulations with data assimilation. Such simulations are not only of interest from a research perspective (e.g., to investigate potential issues that arise when combining (imperfect) models and data in an idealised environment) but can also be viewed alongside the physical set-up in order to enhance the outreach experience.

[More text and literature on flooding and DA etc. See OneNote and proposal. Next steps: FEV illustration, control, etc., for discussion.]

2 Hydraulic model: from kinematic to St. Venant

2.1 River model: open-channel flow

Examples of open channel flow include natural (e.g., rivers and streams) and man-made waterways (e.g., conduits, canals, drainage and sewer systems), in which water flows through channels of varying geometries with a free surface. Fluid mechanical modelling of such flows is termed hydraulic modelling and approximates the three-dimensional problem in a tractable, averaged approach (cf. Te Chow [1959]; Chanson [2004]). Unsteady open channel flow is typically modelled using the St. Venant equations in one (along-channel) spatial dimension with curvilinear along-channel coordinate s. The key variables are: (i) the mean cross-sectional area $A = A(s,t)$ [units m^2] of the river channel, implicitly a function of the mean depth $h = h(s,t)$ [units m] such that $A = A(h,s)$; and (ii) the mean velocity $u(s,t)$. The free sur-

face height [units m] is then defined as the sum of the depth h and bed topography $b = b(s)$ [units m] above zero. Fundamental assumptions of the St. Venant equations are (cf. Chanson [2004]):

- that the flow is hydrostatic, i.e., horizontal length and velocity scales well exceed their vertical counterparts such that vertical fluid accelerations are negligible;
- that flow is one-dimensional, i.e., the transverse free surface is horizontal and the velocity is approximately uniform in a cross-section;
- that channel curvature is small and the bed slope is small, i.e., the angle θ from the horizontal satisfies $\cos\theta \approx 1$ and $\theta \approx \sin\theta$; and
- that sediment and bed motion are neglected on the timescales considered.

Under the first assumption, the two-dimensional depth-averaged shallow water equations (SWEs) can be derived from the primitive equations of motion with horizontal coordinates x and y. The second assumption allows cross-sectional averaging of the two-dimensional SWEs and the St. Venant equations can be derived via the remaining assumptions. Applications are naturally limited by these assumptions. Flow can be strongly non-hydrostatic where there are, e.g., turbulent dynamics, hydraulic jumps, undular bores, and tight bends. The second assumption is not true in flows with cross-channel motions, and also when there is no distinct channel or when multiple channels form. The third assumption does not hold when the channel bed is steep (e.g., mountain streams) or has sharp bends; meandering with a steep bed slope may lead to centrifugal forces acting on the flow, leading in turn to a sloping transverse profile and thereby violating the second assumption. The fourth assumption implies that the effects of sediment transportation on the flow are neglected; further, it does not hold when the channel shifts, e.g., due to erosion.

For the Wetropolis landscape, the spatial coordinate s follows the curved centreline of the main river channel (see Fig. 2). We denote partial derivatives with respect to space and time as $\partial(\cdot)/\partial s := \partial_s$ and $\partial(\cdot)/\partial t := \partial_t$, respectively. The basic St. Venant equations, cf. Chanson [2004]), which solve for the cross-sectional area $A(s,t)$ and along-channel velocity $u(s,t)$, are then

$$\partial_t A + \partial_s(Au) = S_A(s,t), \tag{1a}$$

$$\partial_t u + u\partial_s u + g\partial_s h - g\left(S_o - S_f\right) = 0, \tag{1b}$$

$$h = h(A(s,t), s), \tag{1c}$$

where $S_A(s,t)$ is the mass source term [units $\mathrm{m^2 s^{-1}}$], $S_o = -\partial_s b$ is the bed slope, S_f is the friction term [both dimensionless], and g is the gravitational acceleration [units $\mathrm{ms^{-2}}$]. Note that h appears in (1b) and is known via the (invertible) function (1c) and depends explicitly[1]

[1]Note that explicit dependence on s is needed since $h(A(s_1,t)) = h(A(s_2,t))$ does not imply $s_1 = s_2$. Otherwise said, the cross-sectional area at two locations may be the same, but the depth may differ depending on the channel geometry.

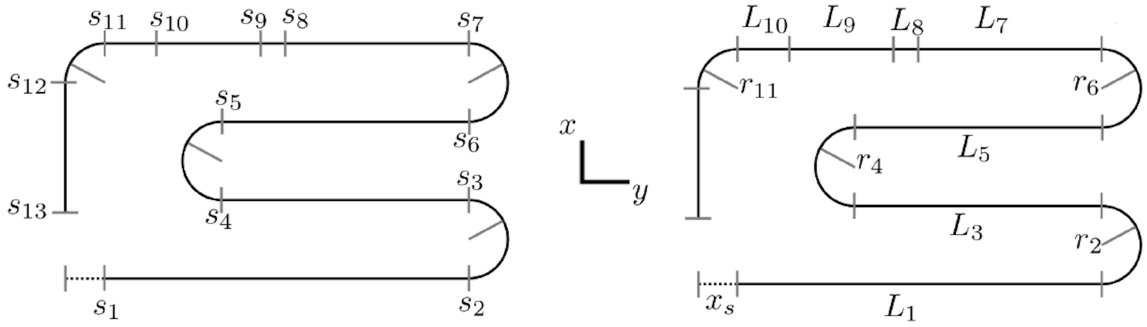

Figure 2: Parameterisation of the river channel in Wetropolis (see Fig. 1) using the along-channel spatial coordinate s. The channel is partitioned into 12 distinct sections $S_i = (s_i, s_{i+1})$ of length $L_i = |S_i|$ for $i = 1, ..., 12$. Radii of curved sections are denoted r_i and x_s is some shift value to move the start location of the river ($s = 0$). [Define $N_s = 12$ since there is an extension possible and useful, using data of only cross-sectional profiles in N_s segments and linking these linearly, say. That would even allows one to deal with real river profiles and non-uniform segments.]

on both $A = A(s, t)$ and s. This system of equations, together with specified initial conditions, upstream and downstream boundary conditions, and lateral inflows, determines how the flow evolves in time. In Wetropolis, mass is added to the river system via random rainfall from the reservoir at s_{res} and the moor at s_{moor}, as well as from canal-1 at s_{1c}; thus, the source term is

$$S_A(s,t) = Q_{res}(t)\delta(s - s_{res}) + Q_{moor}(t)\delta(s - s_{moor}) + Q_{1c}(t)\delta(s - s_{1c}) \tag{2}$$

where Q_{res}, Q_{moor}, Q_{1c} [units $\mathrm{m^3 s^{-1}}$] are the time-dependent inflows (which are determined by separate models for the reservoir, moor, and canal) at their respective locations, and δ is the delta function[2]. [So the delta function carries a unit (or needs a prefactor) of $\mathrm{m^{-1}}$ to reconcile S_A units $\mathrm{m^2 s^{-1}}$ and Q (or Au) units $\mathrm{m^3 s^{-1}}$? Something is amiss here... or I am missing something? Is it because the delta function represents a *point source* so that a volume here is actually an area (volume with infinitesimal width)?] [Think so; one can derive it as limit for real cases of water being fed into a strip. Probably useful to add in an appendix. Yes, cf. your footnote. So derive weak or FV form for a strip and then reason backwards. Also deal with query on/derivation of no along-channel momentum being added.] The friction

[2]While the influx from the moor and reservoir will occur in two strips $s_{moor} - \Delta_{moor}/2 < s < s_{moor} + \Delta_{moor}/2$ and $s_{res} - \Delta_{res}/2 < s < s_{res} + \Delta_{res}/2$, we have assumed Δ_{moor} and Δ_{res} to be small and therefore introduced the river entry points for simplicity via delta functions $\delta(s - s_{moor})$ and $\delta(s - s_{res})$.

term is typically modelled as a function of flow velocity u via the Manning relation:

$$S_f = \frac{C_m^2}{R^{4/3}} u|u|, \tag{3}$$

where $R = R(h) = \frac{\text{wet area}}{\text{wetted perimeter}}$ [units m] is the hydraulic radius and C_m is the Manning friction coefficient. Typically, $C_m \in [0.01, 0.15]$ is empirically derived with higher values meaning higher friction (e.g., $C_m = 0.01$ for flow over asphalt, $C_m = 0.15$ for flow through a "rough" floodplain with trees and foliage); the units of C_m are $\mathrm{m}^{-1/3}\mathrm{s}$. Hence, by combining these terms, the St. Venant equations (1) become

$$\partial_t A + \partial_s(Au) = S_A(s,t), \tag{4a}$$

$$\partial_t u + u\partial_s u + g\partial_s h = -g\left(\partial_s b + \frac{C_m^2}{R^{4/3}} u|u|\right), \tag{4b}$$

$$h = h(A(s,t), s), \tag{4c}$$

with $S_A(s,t)$ given by (2). The domain length is $\sum_{j=1}^{12} L_j = L$ and we define $L_{r1} = \sum_{j=1}^{7} L_j$ and $L_{r2} = \sum_{j=1}^{9} L_j$ [[Put in symbols not numbers]] to be the channel length up to the city area and up to and including the city area, respectively (see Fig. 2). When the continuity equation (4a) is integrated over the domain $[0, L]$, we obtain

$$\frac{\mathrm{d}}{\mathrm{d}t}\int_0^L A\,\mathrm{d}s = Q_{res}(t) + Q_{moor}(t) + Q_{1c}(t) + Q_{s=0}(t) - Q_{s=L}(t), \tag{5}$$

with the (prescribed) inflow $Q_{s=0}(t)$ at $s = 0$ and the (resulting) outflow $Q_{s=L}$ at $s = L$. For subcritical flow[3], the inflow $Q_{s=0} = (Au)\big|_{s=0}$ is given and the outflow set at $Q_{s=L} = (Au)\big|_{s=L}$. [Not quite; characteristics set it. May need some discussion –later.] All Q–fluxes are expressed in $\mathrm{m}^3\mathrm{s}^{-1}$ such that they match the units of the changing volume found on the LHS of (5).

2.1.1 Kinematic model

When the dominant balance on the RHS of (4b) is between the Manning friction and the bed slope or when water depth, bed-slope and velocity are constant, then we can ignore the LHS of (4b), in favour of a kinematic river flow model by using the velocity approximation (e.g., Munson et al. [2009]):

$$u = \frac{R^{2/3}}{C_m}\sqrt{-\partial_s b}, \tag{6}$$

[3]Criticality of the flow concerns the ratio of flow velocity V to the surface (gravity) wave speed c_g, with $c_g = \sqrt{gh}$ in rectangular channels. It is characterised by the (dimensionless) Froude number $\mathrm{Fr} = V/c_g$, with $\mathrm{Fr} < 1$ for subcritical flows and $\mathrm{Fr} > 1$ for supercritical flows.

assuming that u remains positive. This is only valid for subcritical flow (i.e., flow velocity is less than the surface wave speed) and flow in which $h(s,t)$ varies slowly. [Is that true? Exact reduction seems valid as well in all cases?] After substituting (43) into the continuity equation (4a), we obtain the kinematic model:

$$\partial_t A + \partial_s \left(\frac{A R^{2/3}}{C_m} \sqrt{-\partial_s b} \right) = S_A(s,t), \tag{7}$$

with upwind information speed $\mathrm{d}Q(A)/\mathrm{d}A > 0$ for flux

$$Q(A) = Au = A \frac{R(A)^{2/3}}{C_m} \sqrt{-\partial_s b} \quad \text{and inflow} \tag{8}$$

$$A\left(h(s,t),s\right)|_{s=0} = A_0(t). \tag{9}$$

Since $h = h(A(s,t),s)$, (7) is a scalar conservation law in the variable A. Also note that through specification of the inflow discharge $Q_o(t)$ at $s = 0$, $A_0(t)$ can be determined by solving $Q_0(t) = Q(A_0)$ for A_0. This kinematic model (7) has been used to determine suitable time- and length-scales efficiently for design purposes prior to construction of the physical Wetropolis set-up, see Bokhove et al. [2020]. If one wishes to perform accurate predictions of the hydrodynamics in Wetropolis, then more advanced models, e.g., the St. Venant equations, are likely required, in combination with an efficient data assimilation algorithm to constrain the model.

2.1.2 St. Venant equations in conservative form

By combining the mass (4a) and velocity equation (4b), the evolution equation for the momentum, or discharge, Au can be derived:

$$\partial_t(Au) + \partial_s\left(Au^2\right) + \underline{gA\partial_s h} = -g\left(A\partial_s b + \frac{C_m^2 Au|u|}{R(A)^{4/3}}\right) + uS_A(s,t). \tag{10}$$

The conservative form (10) is often used (e.g., Bates et al. [2010]; Borsche [2015]; Hodges [2019]) for two reasons: (i) each term has a clear physical interpretation, and (ii) its structure is appealing from the perspective of finite volume and finite element numerical discretisations. From left to right, (10) can be interpreted as follows: the rate of change of the flow (i.e., discharge) is driven by nonlinear advection, the hydrostatic pressure gradient (via water depth), the gravity down the slope, frictional resistance, and finally any other external forcings.

Noting that the pressure term (underlined above in (10)) is in nonconservative form, it can be expressed (via application of the product rule) as follows:

$$A\partial_s h = \partial_s\left(A\,h\right) - h\partial_s A. \tag{11}$$

This split is desirable because the $A\,h$ term is now in conservative form and the derivative no

longer acts on h directly but on the dependent variable $A = A(s,t)$. Substituting (11) into (10) yields the conservative form of the St. Venant equations (4):

$$\partial_t A + \partial_s(Au) = S_A(s,t), \tag{12a}$$

$$\partial_t(Au) + \partial_s\left(Au^2 + gA\,h\right) - \underline{gh\partial_s A} = -g\left(A\partial_s b + \frac{C_m^2 Au|u|}{R^{4/3}}\right) + uS_A(s,t), \tag{12b}$$

where the nonconservative product has been underlined. [Can one derive 12b from 2D case by width-averaging with inflow at the side?]

Hyperbolic systems of PDEs arise from physical phenomena involving wave motion and/or advective transport. These systems have a rich mathematical structure and are the subject of a wealth of research from both an analytical (e.g., Whitham [2011]) and numerical (e.g., LeVeque [2002]) perspective. To show hyperbolicity and facilitate numerical implementation of the St. Venant system (12), we express it in the following vector form

$$\partial_t \boldsymbol{U} + \partial_s \boldsymbol{F} + \boldsymbol{G}\partial_s \boldsymbol{U} = \boldsymbol{S}, \tag{13}$$

with vector of unknowns $\boldsymbol{U} = \boldsymbol{U}(s,t)$, flux $\boldsymbol{F}$, nonconservative product matrix $\boldsymbol{G}$ and source/sink vector $\boldsymbol{S}$ defined by

$$\begin{aligned} &\boldsymbol{U} = (A, Au)^T, \quad \boldsymbol{F} = \boldsymbol{F}(\boldsymbol{U}) = (Au, Au^2 + g\,h\,A)^T, \\ &\boldsymbol{G} = \boldsymbol{G}(\boldsymbol{U}) = \begin{pmatrix} 0 & 0 \\ -gh & 0 \end{pmatrix}, \quad \boldsymbol{S} = \boldsymbol{S}(\boldsymbol{U}) = \left(S_A, -gA\partial_s b - g\frac{C_m^2 Au|u|}{R^{4/3}} + u\,S_A\right)^T. \end{aligned} \tag{14}$$

The Jacobian matrix $\boldsymbol{J} = \partial\boldsymbol{F}/\partial\boldsymbol{U} + \boldsymbol{G}$ for system (13) is then given by

$$\boldsymbol{J} = \begin{pmatrix} 0 & 1 \\ -u^2 + gA\partial h/\partial A & 2u \end{pmatrix}. \tag{15}$$

The eigenvalues of $\boldsymbol{J}$ are found to be

$$\lambda_\pm = u \pm \sqrt{gA\,\partial h/\partial A} \tag{16}$$

and since $\partial h/\partial A$ is non-negative (see analysis and Figs. 4 and 6 in the following section), we conclude that the system is indeed hyperbolic. There exist novel numerical methods for integrating (nonconservative) hyperbolic systems of PDEs (13); we develop these further for (12) in section 3.

2.2 River model: channel cross-sections

For the Wetropolis landscape and numerical modelling, we consider the invertible functions for the area $A = A(h,s)$, water depth $h = h(A,s)$, topography $b = b(s)$ and hydraulic radius $R = R(h,s)$ along (and as a function of) the spatial coordinate s. When the river water

Table 1: Parameters, their units, and values used in Wetropolis' St. Venant system.

Parameter	Units	Value	Parameter	Units	Value
h_r	m	0.015	L	m	4.2
h_f	m	0.005	g	ms^{-2}	9.81
h_c	m	0.02	C_m	$\mathrm{m}^{-1/3}\mathrm{s}$	0.02
w_r	m	0.05	$\partial_s b$	-	-0.01
w_f	m	0.1	s_m	m	2.038
w_c	m	0.1	s_r	m	0.932

level is sufficiently low, water flows in a rectangular channel with cross-section $A(h,s) = A(s,t) = w_r h(s,t)$ where w_r the (constant) channel width. In that case, the hydraulic radius is $R(h,s) = \frac{w_r h}{2h+w_r}$; alternatively, as a function of area, $R(A,s) = \frac{A}{2A/w_r+w_r}$. When the water level exceeds the top of the rectangular channel, its cross-sectional area depends on its along-channel location s and whether s locates a flood plain or urban area (hence the explicit dependence of h and A on s throughout).

2.2.1 Channel with flood plain

For the channel with a one-sided sloping flood plain, i.e., for $s \in [0, L_{r1} + L_8/2] \cup [L_{r2} + L_{10}/2, L]$, the cross-sectional area is given by:

$$A(h,s) = \begin{cases} w_r h & \text{when } h < h_r; \\ w_r h + \frac{1}{2}\frac{(h-h_r)^2}{\tan\alpha_r} & \text{when } h_r < h < h_r + h_f; \\ h(w_r + w_f) - w_f(h_r + \frac{1}{2}h_f) & \text{when } h > h_r + h_f; \end{cases} \tag{17a}$$

with h_r the main river channel depth, h_f the rise of the flood plain across its width w_f, so that $\tan\alpha_r = h_f/w_f$ where α_r is the angle of slope from horizontal of the flood plain (see Fig. 3). Alternatively, we can invert the above expression to obtain the water depth h as a function of cross-sectional area A:

$$h(A,s) = \begin{cases} A/w_r & \text{when } A < A_1; \\ h_r - w_r\tan\alpha_r + \sqrt{w_r^2\tan\alpha_r^2 + 2(A - w_r h_r)\tan\alpha_r} & \text{when } A_1 < A < A_2; \\ \frac{\left(A + w_f(h_r + \frac{1}{2}h_f)\right)}{w_r + w_f} & \text{when } A > A_2; \end{cases} \tag{17b}$$

with $A_1 = w_r h_r$ and $A_2 = (h_r + h_f)(w_r + w_f) - w_f(h_r + \frac{1}{2}h_f)$. The hydraulic radius is calculated via $R(h,s) = A(h,s)/W(h,s)$, where W is the wetted perimeter:

$$W(h,s) = \begin{cases} w_r + 2h & \text{when } h < h_r; \\ h + w_r + h_r + (h - h_r)\sqrt{1 + \frac{1}{\tan^2\alpha_r}} & \text{when } h_r < h < h_r + h_f; \\ 2h + w_r - h_f + \sqrt{(h_f^2 + w_f^2)} & \text{when } h > h_r + h_f. \end{cases} \tag{17c}$$

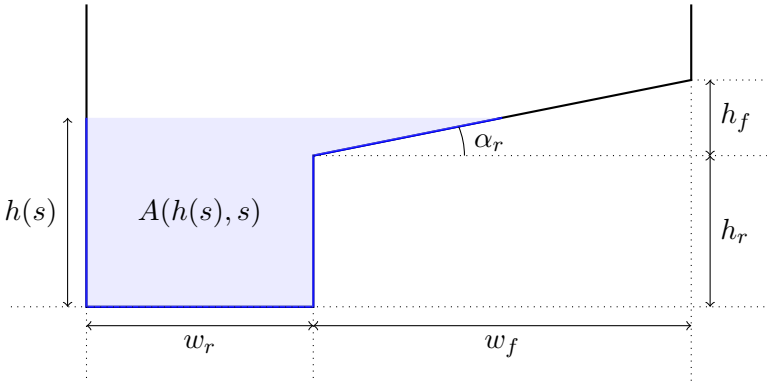

Figure 3: Schematic of the channel geometry with a one-sided sloping floodplain: the cross-sectional area $A = A(h, s)$ (blue shaded area) with associated wetted perimeter $W = W(h)$ (thick blue line), in this instance for $h_r < h < h_r + h_f$ (see equations (17a)–(17c)). When $h < h_r$, the water flows in the rectangular channel of width w_r. Values of the physical Wetropolis channel are given in Table 1.

Finally, since the eigenvalues (16) give wave speed information that is used in the numerical solver, we compute $\partial h/\partial A$ from (17b) as follows:

$$\frac{\partial h}{\partial A}(A, s) = \begin{cases} 1/w_r & \text{when } A < A_1; \\ \frac{\tan \alpha_r}{\sqrt{w_r^2 \tan \alpha_r^2 + 2(A - w_r h_r) \tan \alpha_r}} & \text{when } A_1 < A < A_2; \\ \frac{1}{w_r + w_f} & \text{when } A > A_2. \end{cases} \tag{18}$$

The functions defined above are plotted in Fig. 4 for the parameter values given in Table 1. The domain is split into three regions according to the area and depth thresholds; noteworthy is that all functions are continuous across the thresholds and $\partial h/\partial A$ is positive for all A, thus confirming that the system is hyperbolic in this region (see the previous section and wave-speeds in (16)).

2.2.2 Channel through urban area

The channel in the urban area, i.e., for $L_{r1} + L_8/2 < s < L_{r2} + L_{10}/2$, is flanked by flat rectangular plains which are in turn flanked by vertical walls. Thus, the cross-sectional area is given by:

$$A(h, s) = \begin{cases} w_r h & \text{when } h < h_c; \\ (w_r + 2w_c)h - 2w_c h_c & \text{when } h > h_c; \end{cases} \tag{19a}$$

with w_c is the width of the flat plain (i.e., distance from the main channel to the vertical wall) and $h_c > h_r$ is the river channel depth in the urban area (see Fig. 5). As before, we can invert

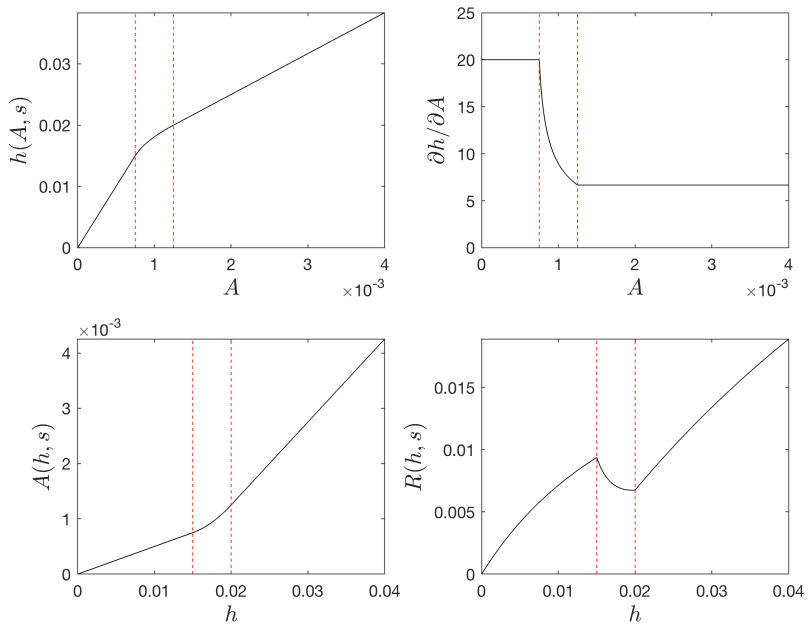

Figure 4: Functional relations for the channel geometry with a floodplain ($s \in \mathcal{L}_{\text{fp}}$; see Fig. 3). Top: h and $\partial h/\partial A$ both as functions of area A (equations (17b) and (18)). Bottom: A and R both as functions of depth h (equations (17a) and R via (17c)). The dotted vertical lines correspond to the threshold areas A_1 and A_2 (top row) and threshold depths h_r and $h_r + h_f$ (bottom row). Geometry parameters are given in Table 1.

the above expression to obtain the water depth h as a function of cross-sectional area A:

$$h(A,s) = \begin{cases} A/w_r & \text{when } A < A_c; \\ \frac{A+2w_c h_r}{w_r+2w_c} & \text{when } A > A_c; \end{cases} \tag{19b}$$

with $A_c = w_r h_c$. As before, the hydraulic radius is calculated via $R(h,s) = A(h,s)/W(h,s)$, where W is the wetted perimeter:

$$W(h,s) = \begin{cases} w_r + 2h & \text{when } h < h_c; \\ w_r + 2w_c + 2h & \text{when } h > h_c. \end{cases} \tag{19c}$$

Finally, from (19b), $\partial h/\partial A$ is given by:

$$\frac{\partial h}{\partial A}(A,s) = \begin{cases} 1/w_r & \text{when } A < A_c; \\ \frac{1}{w_r+2w_c} & \text{when } A > A_c. \end{cases} \tag{20}$$

The functions defined above for the urban area-cross sections are plotted in Fig. 6 for the parameter values given in table 1. The domain is split into two regions according the area

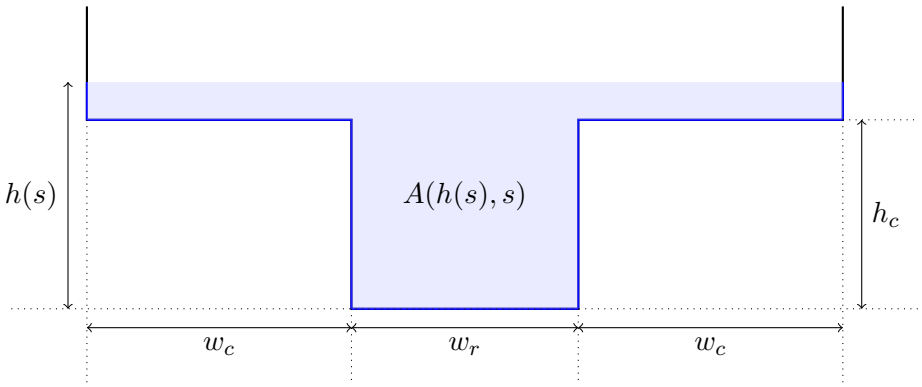

Figure 5: Schematic of the channel geometry in the urban area: the cross-sectional area $A = A(h, s)$ (blue shading) with associated wetted perimeter $W = W(h, s)$ (thick blue line), in this instance for $h > h_c$ (see equations (19a)–(19c)). When $h < h_c$, the water flows in the rectangular channel of width w_r. Values of the physical Wetropolis channel are given in Table 1.

and depth thresholds; sharper transitions across the thresholds mean that $h = h(A, s)$ and $A = A(h, s)$ are continuous but the derivative $\partial h/\partial A$ and hydraulic radius $R(h, s)$ are not. However, $\partial h/\partial A$ remains positive, again confirming that the system is hyperbolic in this region (see previous section and (16)).

2.2.3 Transition between floodplain and urban area

[Implemented in code: choice of linear or smooth (via tanh function) transition from floodplain to city by increasing h_r to h_c over a given length.]

2.2.4 Simplifications

[This section is unchanged from original tex doc in DB – left in for now for reference.]

To simplify matters and to avoid the sudden cross-sectional area changes through the section L_9 and L_{10} in Wetropolis, see Fig. 1, we only use the one cross-sectional river shape but make $h_f = h_f(s), w_f = w_f(s)$ and $h_r = h_r(s)$ smooth functions of s. We also rework $R\left(A, h(A, s), s\right) = R(A, s)$. We therefore adapt the above expressions as follows

$$A(h, s) = \begin{cases} w_r h & h < h_r \\ w_r h + \frac{1}{2}(h - h_r)^2 / \tan \alpha_r & h_r < h < h_r + h_f \\ h(w_r + w_f) - w_f(h_r + \frac{1}{2} h_f) & h > h_r + h_f \end{cases} \tag{21a}$$

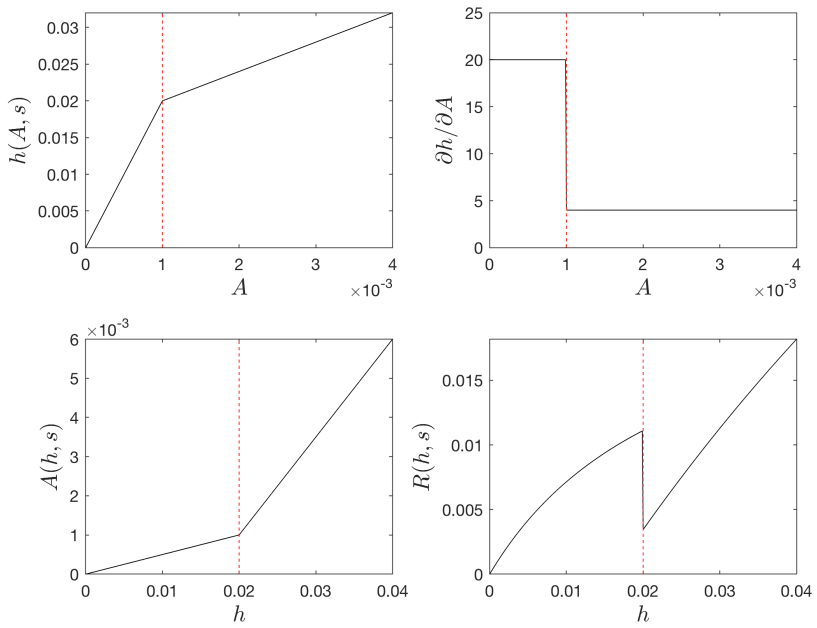

Figure 6: Functional relations for channel geometry in the urban area ($s \in \mathcal{L}_{\mathrm{u}}$; see Fig. 5). Top: h and $\partial h/\partial A$ both as functions of area A (equations (19b) and (20)). Bottom: A and R both as functions of depth h (equations (19a) and R via (19c)). The dotted vertical lines correspond to the threshold area A_c (top row) and threshold depth h_c (bottom row). Channel geometry parameters are given in Table 1.

$$h(A,s) = \begin{cases} A/w_r & A < A_1 \\ h_r + \sqrt{w_r^2 \tan\alpha_r^2 - 2w_r h_r \tan\alpha_r + 2A\tan\alpha_r} - w_r \tan\alpha_r & A_1 < A < A_2 \\ \frac{\left(A + w_f(h_r + \frac{1}{2}h_f)\right)}{(w_r + w_f)} & A > A_2 \end{cases} \tag{21b}$$

$$W(A,s) = \begin{cases} w_r + 2A/w_r & A < A_1(s) \\ (\sqrt{w_r^2 \tan\alpha_r^2 - 2w_r h_r \tan\alpha_r + 2A\tan\alpha_r} - w_r \tan\alpha_r)\times \\ \left(1 + \sqrt{1 + 1/\tan\alpha_r^2}\right) + w_r + 2h_r & A_1(s) < A < A_2(s) \\ \frac{2\left(A + w_f(h_r + \frac{1}{2}h_f)\right)}{(w_r + w_f)} + w_r - h_f + \sqrt{(h_f^2 + w_f^2)} & A > A_2(s) \end{cases}$$

for $s \in [0, L]$ with $\tan\alpha_r = h_f(s)/w_f(s)$, with $A_1(s) = w_r h_r(s)$, $A_2(s) = (h_r(s) + h_f(s))\,(w_r + w_f(s)) -$

$w_f(s)\left(h_r(s)+\frac{1}{2}h_f(s)\right)$ and

$$h_f(s) = \frac{1}{2}h_{f1}\big(2-\tanh\left(a_s(s-L_{r1})\right)-\tanh\left(a_s(L_{r2}+L_{10}-s)\right)\big) - \frac{1}{2}h_{f0}\big(\tanh\left(a_s(L_{r1}-s)\right)+\tanh\left(a_s(s-L_{r2}-L_{10})\right)\big), \tag{21c}$$

$$w_f(s) = \frac{1}{2}w_{f0}\big(2-\tanh\left(a_s(s-L_{r1})\right)-\tanh\left(a_s(L_{r2}+L_{10}-s)\right)\big) - w_{city}\big(\tanh\left(a_s(L_{r1}+L_8-s)\right)+\tanh\left(a_s(s-L_{r2})\right)\big) \tag{21d}$$

$$\begin{aligned} h_r(s) =& h_{r0} + \frac{(h_{wall}-h_{r0})}{2}\left(1+\cos(\pi(s-L_{R1})/l_{fac})\right)\Theta(s-L_{R1}+l_{fac})\Theta(L_{R1}-s) \\ &+ (h_{rc}-h_{r0})\Theta(s-L_{R1}-l_{fac})\Theta(L_{R2}+L_{10}-l_{fac}-s) \\ &+ \left(h_{rc}-h_{r0}+\frac{(h_{wall}-h_{rc})}{2}\left(1+\cos(\pi\frac{(s-L_{R2}-L_{10})}{l_{fac}}\right)\right)\Theta(s-L_{R2}-L_{10}+l_{fac})\Theta(L_{R2}+L_{10}-s) \\ &+ \frac{\left(h_{rc}-h_{r0}+(H_{wall}-h_{rc})}{2}\left(1+\cos(\pi\frac{(s-L_{R1})}{l_{fac}})\right)\right)\Theta(s-L_{R1})\Theta(L_{R1}+l_{fac}-s) \\ &+ \frac{(h_{wall}-h_{r0})}{2}\left(1+\cos(\pi(s-L_{R2}-L_{10})/l_{fac})\right)\Theta(s-L_{R2}-L_{10})\Theta(L_{R2}-L_{10}-s) \end{aligned} \tag{21e}$$

with, e.g., $h_{f1}=0.02$m, $h_{fc}=0.025$m, $w_{f0}=0.1$m, $w_{city}=0.12$m, $h_{r0}=0.15$m, $h_{rc}=0.02$m, $h_{wall}=0.04$m and a smoothing parameter, e.g., $a_s=100$ or $a_s=200$. In addition, we rewrite (**??**) as

$$R(A,s) = A/W(A,s). \tag{22}$$

[Note: this approach with steep and thus large $a_s=100,200$ still seems to give a numerical, artificial peak at the end of the city. It may be an idea to let $h_r(s)$ go up to wall height from its flood-plain-channel height and then to its city height via a berm, thus mimicking the actual finite surrounding wall height in the physical Wetropolis model.]

[could have section with graphs only and some explanation and rest in appendix?]

2.3 Groundwater, canal, and reservoir model

As established in (2), water enters the river channel at moor $s=s_{moor}$ and reservoir $s=s_{res}$ at time-dependent rates $Q_{moor}(t)$ and $Q_{res}(t)$. These rates are determined by models for the groundwater cell (moor) and reservoir (recall Fig. 1), which have been developed in Bokhove et al. [2020] and are coupled here to the St. Venant model for the river dynamics.

2.3.1 Groundwater model

Consider the width-averaged nonlinear diffusion equation modelling groundwater flow in a channel (Barenblatt 1996)

$$\partial_t(w_v h_m) - \alpha g \partial_y(w_v h_m \partial_y h_m) = w_v R/(m_{por}\sigma_e) \tag{23}$$

with groundwater level and variable $h_m = h_m(y,t)$ $[L]$ above a horizontal datum $z = 0$, channel width $w_v \approx 0.1$m, acceleration of gravity $g = 9.81\text{m/s}^2$ $[L/T^2]$, derivative ∂_y in the along-channel direction $y \in [0, L_y]$ of a cell of length $L_y = 0.85$m $[L]$, porosity $m_{por} \in [0.1, 0.3]$, given rainfall rate $R = R(t)$ $[L/T]$, the fraction of a pore $\sigma_e \in [0.5, 1]$ that can be filled with water due to residual air, factor

$$\alpha = k/(\nu m_{por}\sigma_e) \tag{24}$$

with permeability $k \in [10^{-8}, 10^{-9}]\text{m}^2$ $[L^2]$ and viscosity of water $\nu = 10^{-6}\text{m}^2/\text{s}$ $[L^2/T]$. Boundary conditions are no flow at $y = L_y$ such that

$$\partial_y h_m = 0 \tag{25}$$

and a Dirichlet condition at $y = 0$, the other channel end, equal to the water level $h_{cm}(t)$ in a short outflow canal

$$h_m(0,t) = h_{cm}(t). \tag{26}$$

The initial condition is $h_m(y,0) = h_{m0}(y)$. Make a sketch of the situation. The assumptions are that the groundwater level stays underground thus not inducing any surface run-off and that the flow is hydrostatic, with variations in the horizontal y–direction much longer than the vertical length scales. The canal level $h_{cm}(t)$ holds in a short channel of length L_c between $-L_c < y < 0$ with a weir at $y = -L_c$. The water level at the weir is critical, meaning that the flow speed $V_c = \sqrt{gh_c}$ is critical at $y = -L_c$. Assuming stationarity and by using Bernoulli's equation to link the speed and water depth $\{V_{cm}, h_{cm}\}$ in the channel to that at the weir $\{V_c, h_c\}$ one obtains that

$$gh_{cm} + \frac{1}{2}V_{cm}^2 = gh_c + \frac{1}{2}V_c^2 = \frac{3}{2}gh_c \Longrightarrow h_c = \frac{2}{3}h_{cm} \tag{27}$$

assuming in addition that $V_{cm}^2 \ll gh_{cm}$. The critical flux is therefore (see, e.g., Munson et al. 2005):

$$Q_c = w_v h_c V_c = w_v\sqrt{g}\max(2h_{cm}/3, 0)^{3/2}. \tag{28}$$

To obtain further insight, we rewrite and analyse (23) next. The groundwater equation is clearly a continuity equation

$$\partial_t(w_v h_m) + \partial_y(v h_m) = \frac{w_v R}{m_{por}\sigma_e} \tag{29}$$

with the Darcy velocity

$$v = -\frac{kg}{\nu m_{por}\sigma_e}\partial_y(w_v h_m) \tag{30}$$

and Darcy flux

$$\begin{aligned} Q \equiv w_v q \equiv & w_v h_m v = -w_v h_m \frac{\kappa}{\mu}\partial_y p = -w_v h_m \frac{\kappa}{\nu\rho_0}\partial_y p \\ \approx & -\frac{\kappa g}{\nu}\partial_y h_m = -w_v h_m \frac{kg}{\nu m_{por}\sigma_e}\partial_y h_m = -w_v \alpha g \partial_y\left(h_m^2/2\right) \end{aligned} \tag{31}$$

with density of water ρ_0 and where we used the hydrostatic approximation and depth-integration to the free surface at $z = h_m$ by using $\partial_y p/\rho_0 \approx g\partial_y h_m$. The first and last term in (23) display the water balance as follows, in the case that there is no y–dependence:

$$\partial_t h_m = R/(m_{por}\sigma_e). \tag{32}$$

Hence, for h_m zero initially and constant rainfall, we find $h_m = tR/(m_{por}\sigma_e)$ showing that for $m_{por} = \sigma_e = 1$ unity the groundwater level rises directly with rainfall, while it rises faster for general $m_{por} < 1$ and $\sigma_e < 1$, showing that the modelling of rainfall supply is consistent. Hence, the canal level is modelled by the outflow at $y = -L_c$ and inflow at $y = 0$ as follows

$$L_c w_v \frac{\mathrm{d}h_{cm}}{\mathrm{d}t} = m_{por}\sigma_e Q_0 - Q_c \equiv w_v m_{por}\sigma_e \frac{1}{2}\alpha g \partial_y(h_m^2)|_{y=0} - w_v\sqrt{g}\max\left(\frac{2}{3}h_{cm}(t), 0\right)^{3/2}.$$

In summary, the complete mathematical groundwater model is:

$$\partial_t(w_v h_m) - \alpha g \partial_y(w_v h_m \partial_y h_m) = \frac{w_v R}{m_{por}\sigma_e} \quad \text{in} \quad y \in [0, L_y] \tag{33}$$

$$\partial_y h_m = 0 \quad \text{at} \quad y = L_y \tag{34}$$

$$h_m(0,t) = h_{cm}(t) \quad \text{at} \quad y = 0 \tag{35}$$

$$L_c w_v \frac{\mathrm{d}h_{cm}}{\mathrm{d}t} = w_v m_{por}\frac{\sigma_e}{2}\alpha g \partial_y(h_m^2)|_{y=0} - w_v\sqrt{g}\max\left(\frac{2}{3}h_{cm}(t), 0\right)^{3/2} \tag{36}$$

plus initial conditions for h_m and h_{cm}. The multiplication by $m_{por}\sigma$ accommodates the flow out of the groundwater matrix into open space (?), [check for $m_{pro} = 1$!] while the y–derivative of h_m^2 has been taken rather than using $h_m\partial_y h_m$ as otherwise a simple explicit discretisation

with $h_m(0,0) = 0$ is and $h_{cm}(0) = 0$ will not lead to water flux into the canal.

2.4 Summary of overall model

From Bokhove et al. [2020]: The fully coupled system of river, moor and reservoir, including its initial and boundary conditions, for the unknowns $A(s,t)$, $u(s,t)$, $h_m(y,t)$, $h_{res}(t)$, $h_{1c}(t)$, $h_{2c}(t)$ and $h_{3c}(t)$ is as follows [Bokhove et al., 2020] [TO DO: check for consistency... new groundwater model and coupling]:

$$\text{River:} \quad \begin{cases} \partial_t A + \partial_s(Au) = S_A \\ \partial_t(Au) + \partial_s\left(Au^2\right) + gA\partial_s h = -g\left(A\partial_s b + \frac{C_m^2 Au|u|}{R^{4/3}}\right) + uS_A \end{cases} \quad \text{on } s \in [0,L]$$

$$\text{with } h = h(A(s,t)), \quad h(s,0) = h_0(s), \quad u(s,0) = u_0(s),$$

$$\text{and } S_A(t) = (1-\gamma)Q_{res}(t)\delta(s-s_{res}) + Q_{moor}(t)\delta(s-s_{moor}) + Q_{1c}(t)\delta(s-s_{1c}) \tag{37a}$$

$$\text{Moor:} \quad \partial_t(w_v h_m) - \alpha g\partial_y\big(w_v h_m \partial_y h_m\big) = \frac{w_v R_{moor}(t)}{m_{por}\sigma_e} \quad \text{on} \quad y \in [0,L_y]$$

$$\text{with } \partial_t h_m|_{y=L_y} = 0, \quad h_m(0,t) = h_{3c}(t), \quad h_m(y,0) = h_{m0}(y) \tag{37b}$$

$$\text{Reservoir:} \quad w_{res}L_{res}\frac{\mathrm{d}h_{res}}{\mathrm{d}t} = w_{res}L_{res}R_{res}(t) - Q_{res}, \text{ with } h_{res}(0) = h_{r0} \tag{37c}$$

$$\text{Canal–1:} \quad w_c(L_{1c}-L_{2c})\frac{\mathrm{d}h_{1c}}{\mathrm{d}t} = Q_{2c} - Q_{1c}, \text{ with } h_{1c}(0) = h_{10} \tag{37d}$$

$$\text{Canal–2:} \quad w_c(L_{2c}-L_{3c})\frac{\mathrm{d}h_{2c}}{\mathrm{d}t} = Q_{3c} - Q_{2c}, \text{ with } h_{2c}(0) = h_{20} \tag{37e}$$

$$\text{Canal–3:} \quad w_c L_{3c}\frac{\mathrm{d}h_{3c}}{\mathrm{d}t} = \gamma Q_{res} - Q_{3c}, \text{ with } h_{3c}(0) = h_{30}, \tag{37f}$$

$$\text{Influxes:} \quad Q_{1c} = C_f\sqrt{g}\, w_c \max(h_{1c} - P_{1w}, 0)^{3/2} \tag{37g}$$

$$Q_{2c} = C_f\sqrt{g}\, w_c \max(h_{2c} - P_{2w}, 0)^{3/2} \tag{37h}$$

$$Q_{3c} = C_f\sqrt{g}\, w_c \max(h_{3c} - P_{3w}, 0)^{3/2} \tag{37i}$$

$$Q_{moor} = \frac{1}{2} m_{por}\sigma_e w_v \alpha g(\partial_y h_m)^2|_{y=0} \tag{37j}$$

$$Q_{res} = C_f\sqrt{g}\, w_{res} \max(h_{res} - P_{wr}, 0)^{3/2} \tag{37k}$$

as well as hydraulic radius $R(h)$, specified inflow $Q_0(t) = (Au)\big|_{s=0}$, and time-dependent rainfall functions $R_{res}(t), R_{moor}(t)$. The remaining parameters are constants, with units and typical values listed in Table 1. The rainfall functions are defined such that, in the absence of other effects, e.g. unit porosity in the moor, they directly lead to a linear increase of the moor's ground water level and the reservoir depth.

3 Numerical model

3.1 River component

Recall the nonconservative system $\partial_t \boldsymbol{U} + \partial_s \boldsymbol{F} + \boldsymbol{G}\partial_s \boldsymbol{U} = \boldsymbol{S}$ with vector of unknowns $\boldsymbol{U} = \boldsymbol{U}(s,t)$, flux $\boldsymbol{F}$, nonconservative product matrix $\boldsymbol{G}$ and source/sink vector $\boldsymbol{S}$ defined by

$$\begin{aligned}
&\boldsymbol{U} = (A, Au)^T, \quad \boldsymbol{F} = \boldsymbol{F}(\boldsymbol{U}) = (Au, Au^2 + g\,h\,A)^T, \\
&\boldsymbol{G} = \boldsymbol{G}(\boldsymbol{U}) = \begin{pmatrix} 0 & 0 \\ -gh & 0 \end{pmatrix}, \quad \boldsymbol{S} = \boldsymbol{S}(\boldsymbol{U}) = \left(S_A, -gA\partial_s b - g\frac{C_m^2 Au|u|}{R^{4/3}} + u\,S_A \right)^T.
\end{aligned} \tag{38}$$

3.1.1 Space-discretised scheme

The space-discretisation (cf. Rhebergen et al. [2008]; Kent et al. [2017]; Kent and Bokhove [2019]) for this nonconservative system is as follows. We define a mesh (see Fig. 7) on $x \in [0, L]$ with N_{el} cells, nodes x_k with $k = 1, \ldots, N_k + 1$ and cell widths $|K_k| = x_{k+1} - x_k$. In what follows, repeated indices are used for the summation convention with $i, j = 1, 2$ denoting components of vectors; k-subscript denotes values in element K_k; L, R-superscripts and $+, -$-superscripts denote limiting functional values and x values, respectively, to the left/right of an element edge. Instead of the exact Riemann problem, this Godunov-type approach (cf. LeVeque [2002]) uses approximate values of the information speeds $S^{L,R}$

$$\begin{aligned}
S^L &= \min\left(u^L - \sqrt{gA^L \partial h(A^L, s)/\partial A^L}, u^R - \sqrt{gA^R \partial h(A^R, s)/\partial A^R} \right) \quad \text{and} \\
S^R &= \max\left(u^L + \sqrt{gA^L \partial h(A^L, s)/\partial A^L}, u^R + \sqrt{gA^R \partial h(A^R, s)/\partial A^R} \right)
\end{aligned} \tag{39}$$

in order to determine the numerical fluxes $\mathcal{P}^{p,m}$ in the following space-discretised scheme:

$$|K_k| \frac{\mathrm{d}\bar{U}_k}{\mathrm{d}t} = -\mathcal{P}^p(\bar{U}^-_{k+1}, \bar{U}^+_{k+1}) + \mathcal{P}^m(\bar{U}^-_k, \bar{U}^+_k) + |K_k|\bar{S}_k. \tag{40}$$

where left- and right-states are given by $\overline{U}^-_{k+1} = \overline{U}_k$, $\overline{U}^+_{k+1} = \overline{U}_{k+1}$, $\overline{U}^-_k = \overline{U}_{k-1}$, $\overline{U}^+_k = \overline{U}_k$. The numerical fluxes are computed as follows:

$$\mathcal{P}^p_i(\bar{U}^-_{k+1}, \bar{U}^+_{k+1}) = \mathcal{P}^{NC}_i + \frac{1}{2}\int_0^1 G_{ij}(\phi)\frac{\partial \phi_j}{\partial \tau}\,\mathrm{d}\tau, \tag{41a}$$

$$\mathcal{P}^m_i(\bar{U}^-_k, \bar{U}^+_k) = \mathcal{P}^{NC}_i - \frac{1}{2}\int_0^1 G_{ij}(\phi)\frac{\partial \phi_j}{\partial \tau}\,\mathrm{d}\tau, \tag{41b}$$

$$\mathcal{P}^{NC}_i(U^L, U^R) = \begin{cases} F^L_i - \frac{1}{2}\int_0^1 G_{ij}(\phi)\frac{\partial \phi_j}{\partial \tau}\,\mathrm{d}\tau, & \text{if } S^L > 0; \\ F^{HLL}_i - \frac{1}{2}\frac{S^L+S^R}{S^R-S^L}\int_0^1 G_{ij}(\phi)\frac{\partial \phi_j}{\partial \tau}\,\mathrm{d}\tau, & \text{if } S^L < 0 < S^R; \\ F^R_i + \frac{1}{2}\int_0^1 G_{ij}(\phi)\frac{\partial \phi_j}{\partial \tau}\,\mathrm{d}\tau, & \text{if } S^R < 0; \end{cases} \tag{41c}$$

$$F^{HLL}_i = \frac{F^L_i S^R - F^R_i S^L + S^L S^R (U^R_i - U^L_i)}{S^R - S^L}, \tag{41d}$$

where we have suppressed the vector index $i = 1, 2$ of $(\bar{U}_k)_i$ for ease of notation. In the above integrals, $\phi : [0,1] \to \mathbb{R}^n$ is a Lipschitz continuous path, satisfying $\phi(0) = U^L$ and $\phi(1) = U^R$, and connects the model states across the discontinuities arising naturally at the element boundaries in the DGFEM framework [Rhebergen et al., 2008]. Using a linear path $\phi_1 = A_L + \tau(A_R - A_L)$ and low-order numerical Gaussian quadrature for the integration, we find that

$$\begin{aligned} \int_0^1 G_{21}\frac{\partial \phi_1}{\partial \tau}\,\mathrm{d}\tau &= -g\int_0^1 h\left(A^L + \tau(A^R - A^L), s\right)(A^R - A^L)\,\mathrm{d}\tau \\ &\approx -\frac{1}{2}g(A^R - A^L)\Big(h\big(A^L + \frac{1}{2}(1 - 1/\sqrt{3})(A^R - A^L), s\big) \\ &\quad + h\big(A^L + \frac{1}{2}(1 + 1/\sqrt{3})(A^R - A^L), s\big)\Big). \end{aligned} \tag{42}$$

Since the dependency of $h(A, s)$ on s has been enforced previously to be continuous, we can use the value of s at the relevant node in this integral expression.

[Add: initial, boundary data and point source delta functions.]

3.1.2 Preserving the non-trivial steady state solution

When the dominant balance on the RHS of the Au-equation is between the Manning friction and the bed slope, or when water depth, bed-slope and velocity are constant, then we can ignore the LHS of the Au-equation and obtain the kinematic velocity approximation:

$$u^* = \frac{R^{2/3}}{C_m}\sqrt{-\partial_x b}. \tag{43}$$

This is a non-trivial steady-state solution, i.e., flow initialised with constant depth h (and hence cross-sectional area A) and (non-zero) kinematic velocity u^* (43), together with the

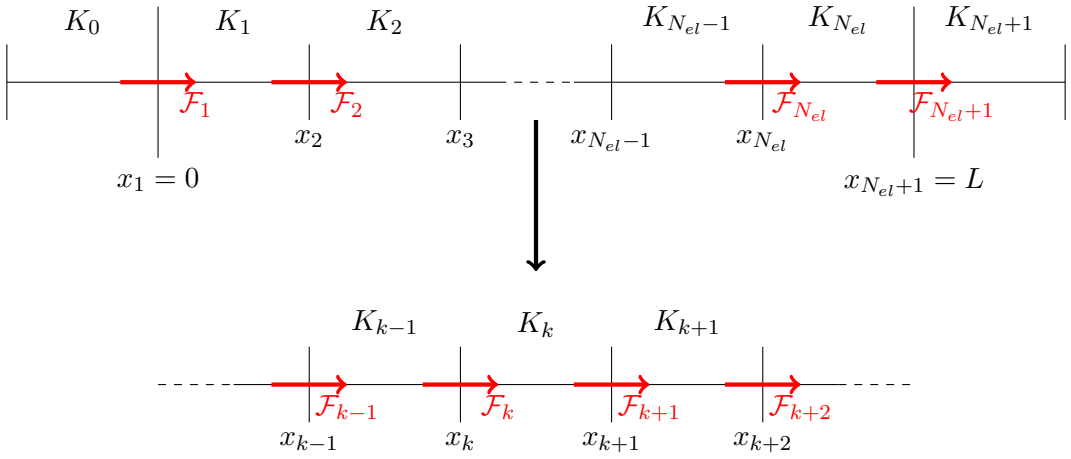

Figure 7: The computational mesh is extended to include a set of ghost elements K_0 and $K_{N_{el}+1}$ to enforce boundary conditions. Central to the DGFEM/FV schemes are the numerical fluxes $\mathcal{F}$ through the nodes, which in this case are given by $\mathcal{P}^{p,m}$ (see eqs. (40) and (41)). For DG0/FV simulations, model variables are projected on to each element K_k as piecewise constant functions, and may be discontinuous across nodes. For DG1 simulations (not shown here), the piecewise linear approximation is used, also discontinuous across nodes.

corresponding kinematic inflow and outflow boundary conditions, is both space- and time-dependent. Here, we show that the space-discretised DG0 (finite-volume) numerical scheme preserves this non-trivial steady state solution numerically for a rectangular channel geometry, i.e., $A = hw_r$ where w_r is the channel width, and constant bed slope $\partial_x b < 0$. Conditions of the steady state are thus:

(SS1) $h^L = h^R$ (equivalently $A^L = A^R$), and

(SS2) $u^L = u^R = u^*$ (so it follows also that $(Au)^L = (Au)^R$).

Recall that the space-DG0 (finite volume) scheme (Eq. 40) for the inhomogeneous system in element K_k reads:

$$0 = |K_k|\frac{\mathrm{d}\overline{U}_k}{\mathrm{d}t} + \mathcal{P}_i^p(\overline{U}_{k+1}^-, \overline{U}_{k+1}^+) - \mathcal{P}_i^m(\overline{U}_k^-, \overline{U}_k^+) + |K_k|\overline{S}_k, \tag{44}$$

where the numerical fluxes are given in Eq. (41) and the left- and right-states are $\overline{U}_{k+1}^- = \overline{U}_k$, $\overline{U}_{k+1}^+ = \overline{U}_{k+1}$, $\overline{U}_k^- = \overline{U}_{k-1}$, $\overline{U}_k^+ = \overline{U}_k$. Recall that we have suppressed the vector index $i = 1, 2$ of $(\overline{U}_k)_i$ and $(\overline{S}_k)_i$ for ease of notation. Noting that $\partial h(A^L, x)/\partial A^L = 1/w_r$ for a rectangular

channel, the numerical wave speeds $S^{L,R}$ (Eq. 39) are:

$$S^L = \min\left(u^L - \sqrt{\frac{g}{w_r}A^L}, u^R - \sqrt{\frac{g}{w_r}A^R}\right) \quad \text{and} \quad S^R = \max\left(u^L + \sqrt{\frac{g}{w_r}A^L}, u^R + \sqrt{\frac{g}{w_r}A^R}\right). \tag{45}$$

The sign of these speeds determines which numerical flux to take in Eq. (41c).

[TO DO: show that, under steady flow conditions (SS1) and (SS2), $S^L < 0 < S^R$ always. Checked numerically: holds for the default set-up. Note that this is the case for the SW trivial steady state solution, since $u = 0$ and $h > 0$, but may not be the case here.

Under the above conditions (SS1) and (SS2) and without loss of generality between left and right states, the numerical speeds are simplified as:

$$S^L = u^* - \sqrt{\frac{g}{w_r}A^L} \quad \text{and} \quad S^R = u^* + \sqrt{\frac{g}{w_r}A^L}. \tag{46}$$

Since u^*, g, w_r, $A^L > 0$, it follows that $S^R > 0$. Less trivial is to show if $S^L < 0$, and whether this is dependent on the parameter values. Considering $S^L < 0$:

$$\begin{aligned} S^L = u^* - \sqrt{\frac{g}{w_r}A^L} < 0 \quad \Longrightarrow \quad A^L &> \frac{w_r}{g}(u^*)^2 \\ &= \frac{w_r}{g}\left(\frac{R(A^L)^{2/3}}{C_m}\sqrt{-\partial_x b}\right)^2 \\ &= \underbrace{\frac{-w_r \partial_x b}{g C_m^2}}_{=:\alpha>0} R(A^L)^{4/3} \end{aligned} \tag{47}$$

where, for a rectangular channel with $A = hw_r$, the hydraulic radius R is given by $R(A) = \frac{\text{wet area}}{\text{wetted perimeter}} = \frac{A}{2A/w_r + w_r}$.

CONCLUSION: Plots of S^L (i) as a function of A for different parameter values and (ii) as a function of a single lumped parameter α for different A values reveal that S^L can be positive under certain parameter combinations. However, this does not lead to unsteady flow... this is because the sign of the numerical speeds does not effect the NCP flux evaluation in (41c). For the 3 inequality cases, the NCP flux $\hat{\mathcal{P}}_i^{NC} = F_i^L = F_i^R$, and so the proof below, which proves steady flow remains steady when $S^L < 0 < S^R$, hold for all 3 cases.]

For $i = 1$ (the A-equation), we have $F_1 = Au$, $S_1 = 0$, and the integral contributions to

(41abc) are zero since $G_{1j} = 0$. Therefore, the HLL-flux (41d) is:

$$F_1^{HLL} = \frac{\overline{Au}^L S^R - \overline{Au}^R S^L + S^L S^R(\overline{A}^R - \overline{A}^L)}{S^R - S^L}$$
$$= \frac{\overline{Au}^L S^R - \overline{Au}^R S^L}{S^R - S^L} = \frac{\overline{Au}^L S^R - \overline{Au}^L S^L}{S^R - S^L} = \overline{Au}^L \frac{S^R - S^L}{S^R - S^L} = \overline{Au}^L = F_1^L \quad \text{since } \overline{A}^R = \overline{A}^L \text{ (SS1)},$$

and the NCP flux is $\hat{\mathcal{P}}_1^{NC} = \mathcal{P}_1^p = \mathcal{P}_1^m = F_1^{HLL} = \overline{Au}^L = F_1^L$. Then:

$$\begin{aligned}
0 &= |K_k| \frac{\mathrm{d}}{\mathrm{d}t} \overline{A}_k + \mathcal{P}_1^p(\overline{U}_k, \overline{U}_{k+1}) - \mathcal{P}_1^m(\overline{U}_{k-1}, \overline{U}_k) + |K_k| \overline{S}_k, \\
&= |K_k| \frac{\mathrm{d}}{\mathrm{d}t} \overline{A}_k + \frac{\overline{Au}_k S_{k+1}^R - \overline{Au}_{k+1} S_{k+1}^L}{S_{k+1}^R - S_{k+1}^L} - \frac{\overline{Au}_{k-1} S_k^R - \overline{Au}_k S_k^L}{S_k^R - S_k^L} \\
&= |K_k| \frac{\mathrm{d}}{\mathrm{d}t} \overline{A}_k + \overline{Au}_k - \overline{Au}_k \quad \text{since } \overline{Au}_k = \overline{Au}_{k+1} \text{ and } \overline{Au}_{k-1} = \overline{Au}_k \text{ (SS2)}, \\
&= |K_k| \frac{\mathrm{d}}{\mathrm{d}t} \overline{A}_k.
\end{aligned}$$

So the cross-sectional area A (and equivalently depth h) is indeed time-dependent: $\mathrm{d}\overline{A}_k/\mathrm{d}t = 0$.

For $i = 2$ (the Au-equation), the flux expressions are more complicated. First of all, the NCP integrals must be evaluated:

$$\begin{aligned}
\int_0^1 G_{2j}(\boldsymbol{\phi}) \frac{\partial \phi_j}{\partial \tau} \mathrm{d}\tau &= -g \int_0^1 h\left(A^L + \tau(A^R - A^L), x\right)(A^R - A^L) \mathrm{d}\tau \\
&= -\frac{g}{w_r} \int_0^1 \left(A^L + \tau(A^R - A^L)\right)(A^R - A^L) \mathrm{d}\tau \\
&= -\frac{g}{w_r}(A^R - A^L)\left[A^L \tau + \frac{1}{2}\tau^2 (A^R - A^L)\right]_0^1 \\
&= -\frac{g}{w_r}(A^R - A^L)\frac{1}{2}(A^L + A^R) \\
&= \frac{g}{w_r} [\![A]\!] \{\{A\}\},
\end{aligned} \tag{48}$$

where we recall that $\{\{\cdot\}\} = \frac{1}{2}((\cdot)^L + (\cdot)^R)$ and $[\![\cdot]\!] = (\cdot)^L - (\cdot)^R$. But since $A^L = A^R$ (SS1) for steady flow, it follows that this integral is zero under such conditions. The flux function is:

$$F_2 = \frac{\overline{Au}^2}{\overline{A}} + g\overline{h}\overline{A} = \frac{\overline{Au}^2}{\overline{A}} + \frac{g}{w_r}\overline{A}^2 \tag{49}$$

and so the numerical fluxes are:

$$F_2^{HLL} = \frac{F_2^L S^R - F_2^R S^L + S^L S^R (\overline{Au}^R - \overline{Au}^L)}{S^R - S^L}$$
$$= \frac{F_2^L S^R - F_2^R S^L}{S^R - S^L} = \frac{F_2^L S^R - F_2^L S^L}{S^R - S^L} = F_2^L \frac{S^R - S^L}{S^R - S^L} = F_2^L \quad \text{since } \overline{Au}^R = \overline{Au}^L \text{ and } F_2^L = F_2^R \text{ (SS1,2)}$$

and $\hat{\mathcal{P}}_2^{NC} = \mathcal{P}_2^p = \mathcal{P}_2^m = F_2^{HLL} = F_2^L = F_2^R$. Finally, the non-zero source term needs evaluating:

$$\overline{S}_k = -g\overline{A}_k \partial_x b - g\overline{A}_k \frac{C_m^2 \bar{u}_k |\bar{u}_k|}{R(\overline{A}_k)^{4/3}} \tag{50}$$

with the kinematic velocity (43). Noting that

$$\bar{u}_k |\bar{u}_k| = \frac{R(\overline{A}_k)^{4/3}}{C_m^2}(-\partial_x b), \tag{51}$$

it follows that

$$\overline{S}_k = -g\overline{A}_k \left(\partial_x b - \frac{C_m^2}{R(\overline{A}_k)^{4/3}} \frac{R(\overline{A}_k)^{4/3}}{C_m^2}(-\partial_x b) \right) = -g\overline{A}_k \left(\partial_x b - \partial_x b \right) = 0. \tag{52}$$

[NOTE: if $\partial_x b$ is not constant, then the $\overline{S}_k$ term may be non-zero and the scheme will not be well-balanced?]

Therefore, considering the evolution of Au in element/volume K_k:

$$0 = |K_k| \frac{\mathrm{d}}{\mathrm{d}t} \overline{Au}_k + \mathcal{P}_2^p(\overline{U}_k, \overline{U}_{k+1}) - \mathcal{P}_2^m(\overline{U}_{k-1}, \overline{U}_k) + |K_k| \overline{S}_k,$$
$$= |K_k| \frac{\mathrm{d}}{\mathrm{d}t} \overline{Au}_k + \frac{F_{2,k} S_{k+1}^R - F_{2,k+1} S_{k+1}^L}{S_{k+1}^R - S_{k+1}^L} - \frac{F_{2,k-1} S_k^R - F_{2,k} S_k^L}{S_k^R - S_k^L}$$
$$= |K_k| \frac{\mathrm{d}}{\mathrm{d}t} \overline{Au}_k + F_{2,k} - F_{2,k} \quad \text{since } F_{2,k} = F_{2,k+1} \text{ and } F_{2,k-1} = F_{2,k} \text{ (SS1,2)},$$
$$= |K_k| \frac{\mathrm{d}}{\mathrm{d}t} \overline{Au}_k.$$

So the momentum Au is time-dependent: $\mathrm{d}\overline{Au}_k/\mathrm{d}t = 0$. We conclude that both A and Au remain constant when initialised with the kinematic flow conditions with a rectangular cross-section and constant bed slope.

3.2 Moor component

3.3 Canal and reservoir components

References

Bates, P. D., Horritt, M. S., and Fewtrell, T. J. (2010). A simple inertial formulation of the shallow water equations for efficient two-dimensional flood inundation modelling. *Journal of Hydrology*, 387(1-2):33–45.

Bokhove, O., Hicks, T., Zweers, W., and Kent, T. (2020). Wetropolis extreme rainfall and flood demonstrator: from mathematical design to outreach. *Hydrology and Earth System Sciences*, 24(5):2483–2503.

Borsche, R. (2015). A well-balanced solver for the saint venant equations with variable cross-section. *Journal of Numerical Mathematics*, 23(2):99–115.

Chanson, H. (2004). *Environmental hydraulics for open channel flows*. Elsevier.

Hodges, B. R. (2019). Conservative finite-volume forms of the saint-venant equations for hydrology and urban drainage. *Hydrology and Earth System Sciences*, 23(3):1281–1304.

Kent, T. and Bokhove, O. (2019). Ensuring well-balanced shallow water flows via the discontinuous galerkin finite element method: issues at lowest order. *Under review: JCP*.

Kent, T., Bokhove, O., and Tobias, S. (2017). Dynamics of an idealized fluid model for investigating convective-scale data assimilation. *Tellus A: Dynamic Meteorology and Oceanography*, 69(1):1369332.

LeVeque, R. J. (2002). *Finite volume methods for hyperbolic problems*, volume 31. Cambridge University Press.

Munson, B. R., Young, D. F., Okiishi, T. H., and Huebsch, W. W. (2009). *Fundamentals of fluid mechanics*, volume 6. Wiley.

Rhebergen, S., Bokhove, O., and van der Vegt, J. J. (2008). Discontinuous galerkin finite element methods for hyperbolic nonconservative partial differential equations. *Journal of Computational Physics*, 227(3):1887–1922.

Te Chow, V. (1959). *Open-channel hydraulics*, volume 1. McGraw-Hill New York.

Whitham, G. B. (2011). *Linear and nonlinear waves*, volume 42. John Wiley & Sons.